



ORIGINAL RESEARCH ARTICLE

# A Theoretical Interpretation of the Experimental Results of an Investigation of the Thermal Expansion Mismatch Strengthening in an Al-Based Metal Matrix Composite Reinforced with Nano-Sized TiCN Particulates

Lubomir Anestiev

Submitted: 25 May 2023 / Revised: 2 November 2023 / Accepted: 26 November 2023 / Published online: 2 January 2024

The coefficient of thermal expansion mismatch (CTEM) strengthening is presumed to be among the main strengthening factors in metal matrix composites reinforced with micro- and nano-sized particulates. It is assumed that the CTEM-generated dislocations obstruct the movement of those generated, when the composite is under external load, thus strengthening the composite. An experimental study, which was carried out on as-produced aluminum-based composite, reinforced with 5 and 10 wt.% nano-sized TiCN particulates (volume fraction of TiCN,  $f_v = 0.0306$  and  $0.0625$ ), failed to detect the predicted by the theory CTEM-generated dislocations. Moreover, it was found that the reinforcement-matrix adhesion forces become weaker with the increase in the reinforcement size. An analysis of the experimental results, intended to investigate the contradiction between the experiment and the postulates of the CTEM strengthening theory, was carried out. The analysis, that implements the dislocation nucleation (Cottrell) and vacancy “drift-diffusion” (Einstein–Smoluchowski) theories, revealed that the classical CTEM strengthening mechanism is active only above a certain, critical size, of the reinforcement. It was found that below that critical size, the composite strength is controlled by the adhesion forces between the reinforcement and the matrix. The theories above predicted that the composite strength (i) would improve as the size of the reinforcement tends to the nano-scale sizes, and (ii) is at its lowest when the size of the reinforcement is commensurate with the aforementioned critical size.

**Keywords** adhesion, CTEM strengthening, dislocations, hot extrusion, metal matrix composites, nanocomposites, vacancies

## Abbreviations

MMC	Metal Matrix Composite
CTEM	Coefficients of Thermal Expansion Mismatch
CDLR	Critical Dislocation Loop Radius
VDRP	Volume Dominated by One Reinforcement Particle
$f_v$	The volume fraction of reinforcement
$w$	The weight fraction of the reinforcement

## 1. Introduction

Metal matrix composites (MMCs), reinforced with ceramic particulates, are promising materials for structural applications, due to the favorable combination of the useful properties of the metal matrix, and the reinforcement (Ref 1-8). The extensive research so far has led to a consensus among the researchers that the reinforcement of an alloy with micron- and/or nano-sized particulates increases its yield and ultimate tensile

strength. However, the factors leading to these improvements, are still an object of debate. An analysis (Ref 9) of the published research on MMCs reinforced with nano-sized particulates, produced by one of the most frequently employed processing methods - hot extrusion, revealed that there is no consensus among the researchers as to which is the strengthening mechanism that leads to composite's strength improvement. Most frequently it is accepted that this improvement is due to, (i) the dislocations generated as a result of the coefficients of thermal expansion mismatch (CTEM), (ii) Orowan's bowing mechanism (Ref 10), and (iii) the Hall-Petch strengthening. Currently, the researchers' preferences are almost equally split between the first two mechanisms, thus adding to the uncertainty of which of those two is the decisive strengthening factor. Bearing in mind the potential application, as structural materials, of the composites, produced by hot extrusion, it is highly desirable to study the strengthening

This invited article is part of a special topical issue of the *Journal of Materials Engineering and Performance* on Residual Stress Analysis: Measurement, Effects, and Control. The issue was organized by Rajan Bhambroo, Tenneco, Inc.; Lesley Frame, University of Connecticut; Andrew Payzant, Oak Ridge National Laboratory; and James Pineault, Proto Manufacturing on behalf of the ASM Residual Stress Technical Committee.

**Lubomir Anestiev**, Institute of Metal Science, Equipment and Technologies with Center for Hydro- and Aerodynamics “Acad. A. Balevski”, Bulgarian Academy of Sciences, 67 Shipchenski Prohod blvd., 1574 Sofia, Bulgaria. Contact e-mail: lanestiev@ims.bas.bg.

mechanisms operating in MMCs reinforced with micro- and nano-sized particles.

The Orowan's bowing mechanism is indeed one of the main strengthening factors in MMCs. It presumes that the strengthening is due to the dislocations' inability to shear through the reinforcement. Hence, Orowan's strengthening is due to the extra force required to bow the dislocation around the reinforcement particle. On the other hand, CTEM presumes that, when a temperature factor is involved, any positive difference between the thermal expansion coefficients of the reinforcement and the matrix would lead to the generation of stresses in the composite, and eventually to the formation of stationary dislocations within the volume dominated by a single reinforcement particle (VDRP). It is assumed that these stationary dislocations would obstruct the movement of those induced by a loading, thus strengthening the composite. It is a confirmed fact, that the employment of the hot extrusion processing method generates stresses in the matrix, due to the relatively rapid cooling of the extrudate. Thus, the composites produced by hot extrusion fulfill the physical prerequisites for strengthening by the CTEM mechanism and do not match those required by Orowan's strengthening mechanism (the temperature factor is missing, etc.). For this reason, we assumed that at the composites, produced by hot extrusion, the CTEM is the main strengthening factor and for this reason, it will be the subject of the present research.

Due to its importance, the CTEM effect was studied intensively. Much of this research, carried out so far, however, is limited to naturally grown (e.g., precipitate-reinforced) or artificially added reinforcements of sizes of tens of microns or above. The effect of nano-sized reinforcement on the mechanical properties of the MMCs is relatively insufficiently well-studied due to the difficulties of the production of these MMCs and the specific experimental methods used in their research. Nevertheless, even this limited research on MMCs reinforced with nano-sized particulates, revealed an interesting feature; the CTEM strengthening effect decreases with the size of the reinforcement and becomes negligible when the size of the reinforcement drops below a certain value. For instance, in a study, Vogt et al. (Ref 7), found that the thermal expansion mismatch effect in a nanostructured metal–matrix composite, synthesized via cryomilling and consolidation, does not occur. According to these authors, this is due to the formation of geometrically necessary dislocations which are constrained to a nanostructured interfacial layer with grains 30–50 nm in size, thus limiting strain hardening in the bulk region of the matrix. It should be noted, however, that in their study the grains were also nano-sized. Sh. Dong, et al. (Ref 8) made a model-aided dislocation-based investigation of the CTEM-absence phenomena. Their investigation, which included the effect of the matrix grain size and reinforcement size on the strengthening in MMCs reinforced with nano/ultrafine-grained carbon nanotubes, revealed that the strengthening decreases with the refinement of the matrix grain size and the size of the reinforcement. These authors attributed those results to the fact that the effect of thermal expansion mismatch strengthening weakens as the reinforcement and the grain size decrease. As a result, the expected strengthening effect is canceled thus making the whole reinforcement procedure meaningless. In a paper (Ref 11), the author et al. also reported the absence of the CTEM strengthening effect in an Al-based MMC reinforced with nano-sized TiCN particulates. It is thus felt, that the problem of the absence of CTEM strengthening at MMCs

reinforced with nano-sized particulates deserves a more detailed study.

This paper aims (i) to investigate the factors behind CTEM strengthening in as-produced MMCs reinforced with nano-sized particulates, and (ii) to establish to what extent and when CTEM could be considered a substantial strengthening factor in such MMCs. For that purpose, an experimental study of the effect of the reinforcement of aluminum with nano-sized TiCN-particulates was carried out, Al-xTiCN ( $x = 5, 10$  wt.%). In addition, a theoretical interpretation of the experimental findings was made. The theoretical analysis, based on the theories of dislocation's nucleation (Cottrell) and vacancy "drift-diffusion" (Einstein–Smoluchowski), revealed how the size of the reinforcement and the applied undercooling during the processing of the composite influence the CTEM strengthening. It was found that (i) CTEM strengthening is activated when the reinforcement sizes exceed a certain, critical size of the reinforcement, and (ii) the CTEM is strongly influenced by the thermo-physical properties of the matrix, which results are in good agreement with those of our experiments.

## 2. Experimental

### 2.1 Materials

The experiments were carried out on aluminum reinforced with 5 and 10 wt.% of nano-sized TiCN particulates (volume fraction,  $f_v = 0.0306$  and  $0.0625$ ). The decomposition of the reinforcement during the processing of the composite was avoided by selecting the powder metallurgy (PM) route; compaction combined with hot extrusion (Ref 11). Commercially available Al powder (Al, min 99.5 wt.%; Fe, max. 1 wt.% with a mean particle diameter of  $\sim 37 \mu\text{m}$ ) and TiCN (nano-sized powder with a mean radius of the particles,  $\langle r_p \rangle \cong 15\text{--}25$  nm) were used as base powders. After the mechanical mixing, the powder mixture was subjected to a 10-min mill and mix (M&M) procedure in a planetary agate ball mill. The specific conditions applied were: room temperature, the total weight of the powder mixture – 160 g, inert gas atmosphere (Ar), a rotating speed – 500 rpm, ball weight to powder weight ratio (BPR) – 0.4225, and the total weight of the balls – 67.6 g. The purpose of the M&M procedure was to prevent the liquation (respectively, the accompanying agglomeration) of the reinforcement, by embedding the TiCN particles onto the Al powder surface, thus ensuring easy handling of the green powder during subsequent processing and a homogeneous distribution of the reinforcement throughout the samples.

### 2.2 Processing of the Green Powders

The as-prepared green powders were shaped into rods by cold isostatic pressing at different compacting pressures. These bars were hot extruded, extrusion ratio 6:1, at temperatures varying between 0.8 and 0.85 of the aluminum melting temperature (RUE 250 SS hydraulic press supplied with a mold heater and molds allowing a variable degree of reduction). The hold time of the extrudates in the mold was up to 20 min, which ensured: (i) equalizing the temperature through the mold-extrudates assembly, and (ii) degassing of the pre-pressings. The friction between the mold and the extrudates was reduced by applying a high-pressure lubricant, "Vapor". Achieving a product free of reinforcements' agglomeration and high density,

and a small-grained structure was accomplished by varying the processing parameters. The optimum of the extrudates quality was achieved at; cold compaction at 600 MPa, holding time under load 1 min, and hot extrusion at  $T_{\text{extr}} = 470 \pm 10$  °C, lasting 10 min, with a subsequent cooling in air. The extrudates, rods of 12 mm in diameter, were cut into pieces, approximately 70 mm in length, to be further formed into test samples. All experiments were carried out on samples made from the as-produced MMCs, i.e., without these being subjected to additional processing and/or treatment.

### 2.3 Experimental Methods

The microstructure of the specimens in this research was studied by scanning electron microscopy (SEM/FIB LYRAI XMU, TESCAN) equipped with an EDX detector (Quantax 200, Brücker) and transmission electron microscopy (TEM/ JEOL-JEM 1011, 100 kV). The SEM specimens were prepared using conventional grinding and polishing techniques; wet grinding (grinding paper No. 3000), mechanical polishing with diamond paste, and etching with a 0.5 % water solution of Hydrofluoric acid (Ref 11) at room temperature. The TEM specimens were prepared from plates (thickness  $\sim 700$   $\mu\text{m}$ ) sliced from the test samples, which were mechanically thinned to foils of 20-30  $\mu\text{m}$  by grinding (grinding paper, F2000) and final polishing with diamond paste (Struers DP P-1  $\mu\text{m}$  paste). From the as-prepared foils were formed discs, 3 mm in diameter, which were subsequently electrolytically polished at room temperature (Struers Tenupol Electropolisher, operating at 15 V) in a solution of 20%  $\text{HClO}_4$  and 80 %  $\text{CH}_3\text{COOH}$ .

### 2.4 Results

The results obtained from the TEM and SEM study of the MMCs are shown in Fig. 1(a), 2, and 3 (Ref 13). Figure 1(a) shows a TEM micrograph taken from an as-prepared sample. According to the CTEM theory, the generated dislocation density,  $\rho_{\text{CTE}} = \frac{6\Delta\alpha\Delta T f}{b(r_0)(1-f)}$  (Ref 12) for a temperature difference  $\Delta T \cong 400$  K, Burger's vector  $b \approx 0.25$  nm, a CTE-mismatch of  $\Delta\alpha \cong 2.10^{-6}$   $\text{K}^{-1}$ , and an adhesion parameter of  $f \sim 0.5$  should be  $\sim 200$  dislocations per  $\mu\text{m}^{-2}$ . That is the micrographs in Fig. 1(a) and (b) should show similar dislocation density patterns—dense dislocation networks around the reinforcement particles. As seen this is not the case. (Note: The micrograph shown in Fig. 1(b) is not related to the present research and is added for illustrative purposes only.) It should be noted that tilting the specimen up to 8° in all directions and switching from bright to dark field mode also failed to detect dislocations in the studied specimen. That is, for some reason, the CTEM failed to produce detectable dislocation density around the nano-sized reinforcement particles. On the contrary, as reported in (Ref 6, 14, 15), the micron-sized reinforcement particles show readily detectable dislocation loops in their neighborhood. Whence, taking into account the already cited research of Vogt et al. and Sh. Dong, et al., it follows that CTEM should be a reinforcement-size-sensitive phenomenon, cf. the Introduction section.

Further, the analysis of the SEM micrograph, Fig. 2 shows that reinforcement particles of different sizes are not equally strongly attached to the Al-matrix. For instance, at the center in Fig. 2, a micron-size TiCN particle has detached from the matrix, see the cavity at the center, while those with smaller

sizes stay firmly embedded in it. Therefore, for some reason, the micron-sized particles are much easier to separate from the matrix than those with lesser sizes. The rough contact surface of the bed cavity leads to the conclusion that the bonds that keep the reinforcement-matrix construct together have failed. As the specimen was not tensionally loaded, the unbinding should have taken place during the cooling of the specimen. In our case,  $\Delta\alpha > 0$ , whence, the only possible explanation is to presume that the vacancies and/or the dislocations present in the matrix have piled up near, or even annihilated into the reinforcement-matrix contact zone, thus reducing the adhesion. If this is the case, then the observed in Fig. 2 brighter rings around the reinforcements, are readily explained by the higher intensity of the  $e$ -beam reflected from the reinforcement's surface. This is feasible only if these places are much easier penetrable by the  $e$ -beam. To confirm, or reject, the preceding conclusion a relatively large particle in a studied sample was selected, cf. Fig. 3. The readily noticed brighter ring around the particle suggests much easier penetration of the  $e$ -beam through these parts, which could be explained only with an increased concentration of vacancies and/or dislocations in those parts (Ref 11). Therefore, the conclusions made above are completely justified.

Evaluation of the CTEM pressure  $P$ , acting on the matrix-reinforcement interface, shows that it exceeds the yield stress,  $\sigma_Y$ , of the matrix (here Al) for all reinforcement sizes and processing temperatures. Thus, a shell of a plastically deformed zone should be detectable around every reinforcement particle (Ref 16-18). Again, this is not the case, which agrees with the contemporary concepts; plastic deformation in metals occurs only if a certain concentration of dislocations is available, see, e.g., (Ref 18, 20).

## 3. Discussion

The analysis carried out below aims to reveal how the reinforcement size, and possibly the applied undercooling at the processing of the composite, affect the CTEM-induced strengthening. For that purpose the following conventions and assumptions were used; (i) at the micron-level, the metal always performs as elastic, (ii) plasticity occurs only when a sufficient number of dislocations is available (Ref 6, 18), (iii) the reinforcement has a spherical shape, (iv) CTEM causes in the matrix the same deformation as a pressurized cavity inflicts in an infinite elastic medium (Ref 16, 17), (v) the reinforcement is unyielding.

The absence of dislocations when utilizing nano-sized reinforcements (Fig. 1a) and their presence when micron-sized reinforcements are employed (Ref 6, 14), suggests that the origin of this difference should be sought in the factors controlling the dislocations' genesis. To solve the problem at hand we rely on a theory developed by Cottrell (Ref 15, 20). In his theory, Cottrell argues that it is impossible to nucleate a viable loop (i.e., circular-shaped) dislocation, whose radius is less than some critical value. Denoted from here on as, critical dislocation loop radius (CDLR). To determine CDLR, Cottrell proposed to minimize the difference between the energy required to form a loop dislocation with radius  $r$ , that is,  $\frac{Eb^2(1-\nu/2)r}{4(1-\nu)(1+\nu)} \ln\left(\frac{r}{2b}\right)$  (Ref 21, 22), and the excess energy, that is gained from the applied stress,  $\pi r^2 b \tau$ .



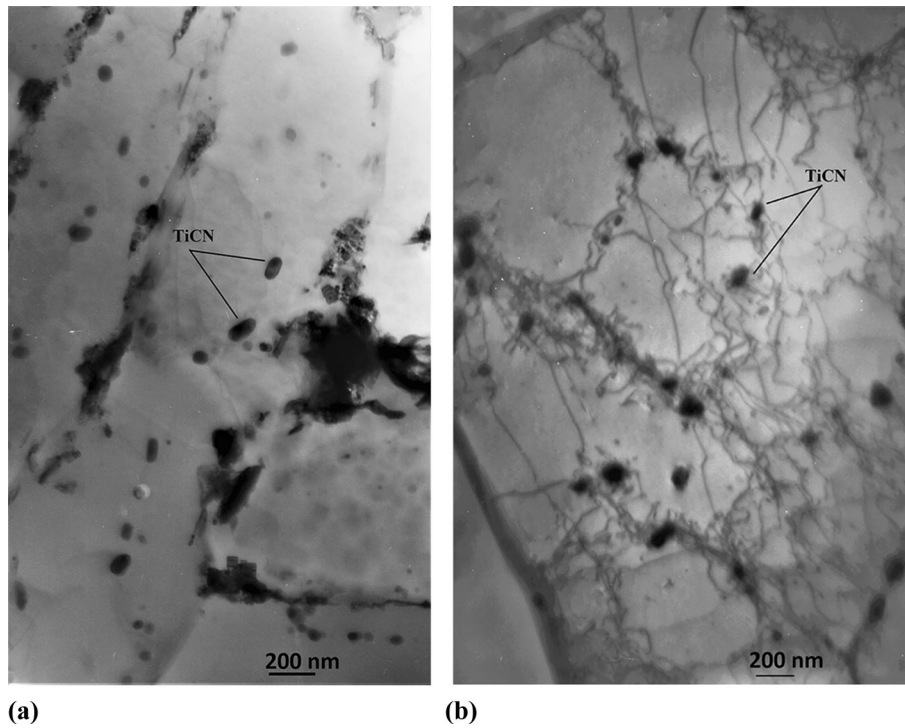


**Fig. 1** TEM micrographs (Ref 13) of two specimens reinforced with 10 wt.% TiCN ( $f_v = 0.0625$ ). (a) specimen prepared from an as-produced sample, (Fig. 1b) specimen made from a test piece subjected to tensile loading, (overall strain,  $\epsilon = 0.08$  (8%) (Ref 11), the micrograph is taken from a plastically deformed part of the test piece). (b) is included for comparison purposes only. It is intended to illustrate how the surroundings of reinforcement particles would look if CTEM strengthening is active

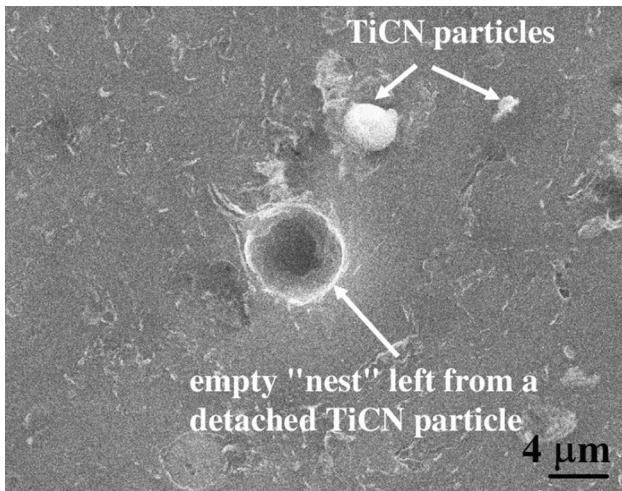


**Fig. 2** An SEM image (Ref 13) of a TEM foil, made from an as-produced reference sample, showing reinforcement particles of different sizes (weight fraction of the reinforcer,  $w = 10$  wt.% TiCN,  $f_v = 0.0625$ ). Notice the differences in the reinforcement-matrix interaction behavior, depending on the size of the reinforcer

The minimization procedure yielded for the CDLR:

$$r_c = \frac{Eb(1-v/2)}{4\pi(1-v)(1+v)\tau} \left[ \ln\left(\frac{r_c}{2b}\right) + 1 \right] \\ = \frac{Eb(1-v/2)}{4\pi(1-v)(1+v)\tau} \ln\left(\frac{r_c e}{2b}\right). \quad (\text{Eq 1})$$

Here  $r_c$  denotes the CDLR in [m],  $E$  and  $\nu$  are the Young modulus [Pa] and the Poisson ratio of the matrix,  $\tau$  is the resolved shear stress, and  $e$  is the natural logarithms base.

By making use of the well-known instance from the theory of elasticity,  $\tau = \frac{\sigma_{\phi\phi} - \sigma_{rr}}{\sqrt{3}}$ , and keeping in mind that the stresses generated within an infinite elastic media by a pressure,  $P$ , applied to the internal wall of a pressurized cavity are,  $\sigma_{\phi\phi} = P/2\rho^3$  and  $\sigma_{rr} = -P/\rho^3$  (Ref 10), for the resolved shear stress is obtained,  $\tau = \frac{mP\sqrt{3}}{2} \left(\frac{\langle r_p \rangle}{r}\right)^3$ . Where  $\langle r_p \rangle$  denotes the mean radius of the reinforcement,  $\sigma_{\phi\phi}$  and  $\sigma_{rr}$  are the components of

the stress tensor in spherical coordinates,  $r$  is the distance from the center of the reinforcement, and  $m$  is the Schmid factor (Ref 23), introduced here to account for the spatial orientation of the glide planes and the slip directions of the dislocations generated. Bearing in mind that the CTEM-induced pressure on the inner wall of the matrix-reinforcement contact zone is,  $P = 2E\Delta\alpha\Delta T/(1+\nu)$ , for the resolved shear stress generated by the CTEM is finally obtained,  $\tau = \frac{m\sqrt{3}E\Delta\alpha\Delta T}{2} \left(\frac{\langle r_p \rangle}{r}\right)^3$ . Thus,

introducing new dimensionless variables,  $\rho = r/\langle r_p \rangle$ ,  $\rho_c = r_c/\langle r_p \rangle$ , and substituting in (1)  $\tau$  with its equal, is obtained:

$$\rho_c = \frac{b(1-v/2)\rho^3}{4m\sqrt{3}\pi(1-v)(1+v)\Delta\alpha\Delta T\langle r_p \rangle} \left[ \ln(\rho_c) + \ln\left(\frac{e\langle r_p \rangle}{2b}\right) \right]. \quad (\text{Eq 2})$$

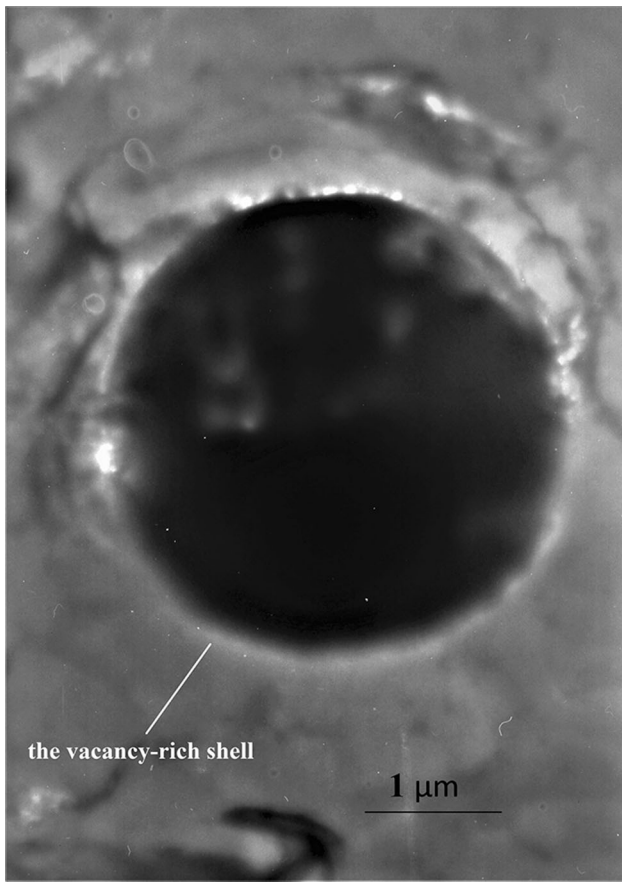


**Fig. 3** TEM micrograph (Ref 13) taken from a specimen prepared from an as-produced sample reinforced with 5 wt.% TiCN, ( $f_v = 0.0306$ ). Notice the excess thinning of the Al-matrix in the neighborhood of that large reinforcement particle (the bright halo around the particle). This thinning is attributed to the excess of vacancies in this zone. The thickness of the vacancy-rich shell around the particle is estimated to be 1/12 -th of the particle's radius

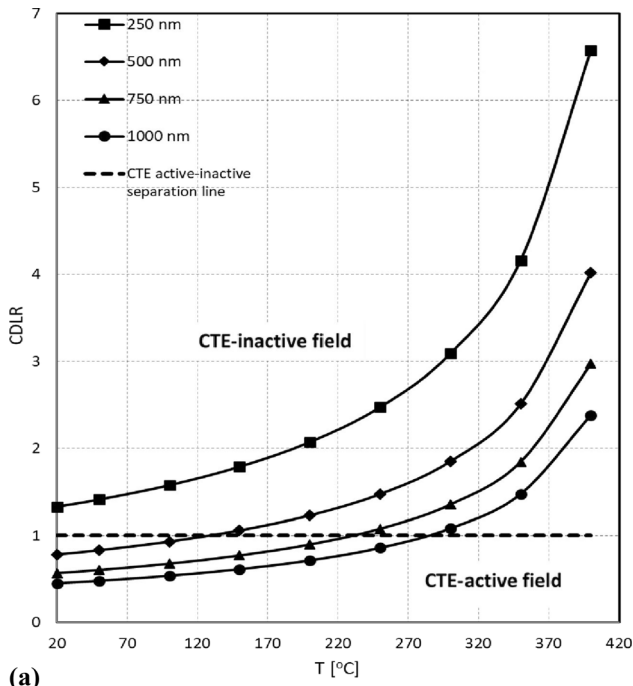
Because the glide planes and the slip directions of the dislocations are randomly oriented in space, in the calculations below we use an average value of the Schmid factor,  $m = 0.25$ ).

Analysis of Eq 2 shows that the dimensionless CDLR,  $\rho_c$ , is inversely proportional to the size of the reinforcement,  $\langle r_p \rangle$ ; the decrease in the reinforcement size,  $\langle r_p \rangle$ , thus, would lead to the increase in the CDLR size, while an increase would lead to its reduction. The fact that CDLR is inversely proportional to the resolved shear stress  $r_c \sim \tau^{-1}$  (cf. Eq 1) indicates that the places with higher stress intensity, such as the neighborhoods of the reinforcement, possess the highest chance of generating viable dislocations. On the contrary, the lower the stress intensity the larger is CDLR, and the less probable its nucleation. Remind, that a larger CDLR requires a larger amount of nucleation work which must be, in our case, provided from the stress induced by the CTEM. Under the preceding, the chances of nucleating a viable CDLR drops with the distance from the reinforcement proportionally to,  $\rho^3$ , i.e., very fast. Cottrell's theory, therefore, leads to the conclusion that viable dislocations would nucleate predominantly in the neighborhood of the reinforcement and that their sizes should be commensurate with the size of the reinforcement particle, cf. (Ref 6, 14). Based on the preceding it follows: (i) When the size of the reinforcement is larger than the CDLR,  $r_c / \langle r_p \rangle < 1$  ( $\rho_c < 1$ ), the CTEM strengthening mecha-

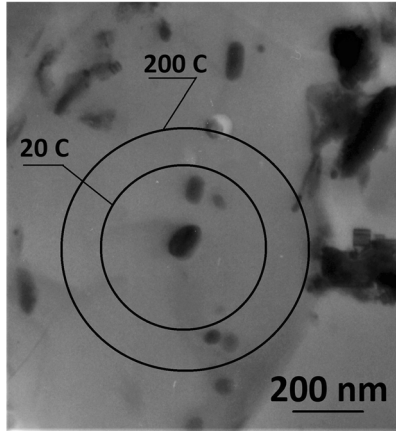
nism is operational and the generated dislocation loops are energetically stable; (ii) Because of the CTEM stress gradient around of the reinforcement, the as-nucleated dislocations are pushed from the reinforcement toward the interparticle space (Ref 6, 12-15), thus, forming dislocation clusters at the VDRP boundaries, which, as reported by Vogt et al., eventually serve as barriers to the movement of the load-generated dislocations; (iii) The critical reinforcement radius below which the CTEM strengthening mechanism becomes non-operational is thus determined by the identity,  $r_c / \langle r_p \rangle \approx 1$  ( $\rho_c \approx 1$ ). Hence, the reinforcement radius at which CTEM strengthening ceases to be operational is determined by the transcendental equation,  $\langle r_p \rangle = \frac{b(1-\nu/2)}{4m\sqrt{3}\pi(1-\nu)(1+\nu)\Delta\alpha\Delta T} \ln\left(\frac{e\langle r_p \rangle}{2b}\right)$ ; (iv) The CDLRs whose radii are larger than that of the reinforcement,  $r_c / \langle r_p \rangle > 1$  ( $\rho_c > 1$ ), are energetically unstable and will eventually decompose to vacancies. The dislocations' disintegration time depends on the self-diffusion coefficient of the matrix atoms and for Al it was estimated to be  $\sim 80$ -100 s (Ref 24).

The theory, Eq 2, is illustrated by applying it to an aluminum-based MMC reinforced with TiCN (cf. Fig. 4a, and b). The calculations were carried out at,  $\rho = 1$ ,  $\Delta\alpha = 2.10^{-6}$  (Ref 25),  $\nu_{Al} = 0.345$  (Ref 26), and  $b \approx 0.25$  nm (Ref 11). Recall that  $\rho = 1$  (the vicinity of the reinforcement particle) is the maximum-stressed part of the matrix, thus, the most probable place where a dislocation could be nucleated. Figure 4(a) shows plots of the calculated dimensionless CDLRs vs.  $\Delta T$ , obtained by varying in (2) the size of the reinforcement. (Recall that,  $\Delta T = T_{extr} - T$ , is the difference between the processing and an arbitrary temperature  $T$ ). The dashed line in Fig. 4(a) marks,  $\rho_c \approx 1$ , i.e., the boundary separating the operational and non-operational fields of the CTEM strengthening. Figure 4(b) illustrates the proportions between the sizes of a reinforcement particle,  $\langle r_p \rangle \sim 30$  nm (this is the particle at the center of Fig. 1a), and the generated by it CDLRs at two arbitrary final processing temperatures, 20 °C ( $\Delta T = 450$  °C) and 200 °C ( $\Delta T = 270$  °C). As seen these are larger than the size of the particle, thus according to the preceding discussion, no dislocation loops could be nucleated and observed around that specific particle, which is in agreement with the experimental evidence, cf. Fig. 1(a) and the discussion in the Results section.

The results so far, theory and experiment, show that CTEM, as a strengthening mechanism, is not operational in the whole reinforcement-sizes range. Regardless of the reinforcement's size, however, the CTEM will always induce stress and it is not quite clear how it is affecting the strength of the composite. Therefore, it is desirable to extend the present analysis to reinforcement sizes below the critical, thus clarifying how the composite strength would be affected. The experimental fact that particles with sizes less than the critical do not separate from the matrix (see the previous section) suggests that the reduction of the reinforcement sizes from micron- to nano-scale ones does not negatively affect the binding (adhesion) forces acting on the matrix-reinforcement interface (Ref 27). Thus, bearing in mind the experimental facts and recalling that the reduction of the reinforcement size strongly influences the stress induced by CTEM, it is reasonable to assume that the particle size affects the adhesion forces in the same way. Because these forces are negatively affected by crystal lattice defects, e.g. the accumulation of vacancies near the matrix-reinforcement contact zone, it could be readily assumed that the



(a)



(b)

**Fig. 4** (a) Calculated with Eq 2 CDLRs as a function of the temperature and reinforcement sizes. The field enclosed between the dashed line and the abscissa indicates the operational field of the CTEM strengthening. (b) Calculated with Eq 2 CDLRs for two arbitrary final processing temperatures, 20 °C ( $\Delta T = 450$  °C) and 200 °C ( $\Delta T = 270$  °C) compared with the size of the particle,  $\langle r_p \rangle \sim 30$  nm that produces the stress field (cf. the central particle in Fig. 1a  $w = 10$  wt.% TiCN,  $f_v = 0.0625$ ). By the large size of the CDLRs is readily deduced that the stress field intensity produced by that particle is insufficient to produce viable dislocation loops that satisfy the criterion formulated in the text, hence, the lack of dislocations in the vicinity of that particle in Fig. 1a

observed increase/decrease in their strength is due to the vacancies' concentration (aka "the site fraction of monovacancies") near that zone. According to a principle formulated by Le Chatelier and Braun (Ref 28), in a stress field, the vacancies should diffuse in a direction that would reduce the stress gradient. In our case, that is toward the stress-generating center, the reinforcement particle. The stress decrease, however, would affect negatively the composite strength, due to the increase in the vacancy concentration near the matrix-reinforcement con-

tact zone. The stationary distribution of the vacancies in a stress field could be determined by employing an equation proposed by Einstein and Smoluchowski (Ref 29), which in spherical coordinates reads:

$$\frac{dC_v}{d\rho} = -\frac{C_v}{k_B T} \frac{dU}{d\rho}. \quad (\text{Eq 3})$$

Here  $k_B$  is the Boltzmann constant,  $C_v = C_v(\rho)$  is the vacancy concentration,  $U(\rho)$  is the stress potential [J], and  $\rho$  is as above, the dimensionless distance from the center of the reinforcement.

Because we deal with reinforcements whose radii are less or around a micron, the convention (i) of this section applies. That is the potential gradient,  $dU/d\rho$ , could be evaluated by employing the theory of elasticity. We remind that  $dU/d\rho$ , depends on the stress-energy intensity,  $u(\rho) - dU/d\rho = 4\pi\rho^2 u(\rho) \langle r_p \rangle^3$  (Ref 16, 17). Bearing in mind that the CTEM-generated stress-energy intensity depends on the pressure exerted on the matrix by the reinforcement as,  $u(\rho) = 3P^2(1+\nu)/E\rho^6 \text{ Jm}^{-3}$  (Ref 16) and recalling that this pressure is equal to,  $P = 2E\Delta\alpha\Delta T/(1+\nu)$ , it is readily obtained,  $dU/d\rho = 48\pi E(\Delta\alpha\Delta T)^2 \langle r_p \rangle^3 / (1+\nu)\rho^4$ . Regrettably, the dependency of the Young modulus on the vacancy concentration,  $E(C_v)$ , is unknown. In this research this difficulty is overcome, by presuming that the vacancies form a binary solution with the matrix atoms, an approach widely used in the theory of self-diffusion (Ref 30-32). By employing the formalism of the thermodynamic theory of solutions (Ref 33) and neglecting the partial contribution of the vacancies in that solution, as insignificantly small, is obtained,  $E(C_v) \cong \bar{E}_m(1 - C_v)$ , with  $\bar{E}_m$ , as the partial Young modulus of the matrix (cf. the Appendix). We note that,  $\bar{E}_m$ , also depends on the vacancy concentration. Still, the problem could be made tractable, by declaring,  $\bar{E}_m$ , a parameter depending on the average vacancy concentration in the vicinity of the reinforcement,  $\bar{C}_v$ , that is  $\bar{E}_m \approx \bar{E}_m(\bar{C}_v) = \text{const.}$  Whence, replacing in (3)  $E(C_v)$  and  $dU/d\rho$  with their equal yields:

$$\frac{dC_v}{d\rho} = -\frac{48\pi\bar{E}_m(\bar{C}_v)(\Delta\alpha\Delta T)^2 \langle r_p \rangle^3 C_v(1 - C_v)}{k_B T(1 + \nu)\rho^4}, \quad (\text{Eq 4})$$

The boundary condition at the VDRP boundary is,  $C_v(\rho_Y) = C_0$ , where  $C_0$  is the vacancy concentration,  $\rho_Y = \left[1 + \frac{d_r}{d_m} \left(\frac{100}{\text{wt.}\%} - 1\right)\right]$  is the outer radius of the VDRP,  $d_r$ , and  $d_m$ , are the densities of the reinforcement and the matrix, and wt.% is the weight fraction of the reinforcement in %. Presently, we will need the value of VDRP in an aluminum composite reinforced with 5 wt.% TiCN ( $f_v = 0.0306$ ). Thus, replacing,  $d_r$  with  $4 \text{ gcm}^{-3}$  (Ref 34), and  $d_m$  with  $2.7 \text{ gcm}^{-3}$  into the instance above for that VDRP radius is obtained,  $\rho_Y = 3.13$ . The introduction of a dimensionless parameter,  $k = 16\pi\bar{E}_m(\bar{C}_v)(\Delta\alpha\Delta T)^2 \langle r_p \rangle^3 / (1 + \nu)k_B T$ , allows rewriting (4) in a more compact form:

$$\frac{dC_v}{d\rho} = -\frac{3kC_v(1 - C_v)}{\rho^4}. \quad (\text{Eq 4a})$$

Eq 4a, after the boundary conditions are accounted for, solves to:

$$C_v(\rho) = C_0 \exp\left(k\left(\frac{1}{\rho^3} - \frac{1}{\rho_Y^3}\right)\right) / \left[1 + C_0 \exp\left(k\left(\frac{1}{\rho^3} - \frac{1}{\rho_Y^3}\right)\right)\right]. \quad (\text{Eq 5})$$



The dimensionless parameter  $k$  allows for obtaining a unified solution to the vacancy concentration distribution problem. That is, when the value of  $k$  is determined for a specific pattern of vacancy distribution, other solutions, valid for this specific distribution pattern, could be readily obtained by varying the parameters/constants included in  $k$ .

Regrettably,  $k$  is unknown and so is,  $\bar{E}_m(\bar{C}_v)$ . However, it could be estimated by matching the calculated with an experimentally determined vacancy distribution. Because in the present research, the latter is unavailable, a rough estimate of the parameter  $k$  was obtained by using as an indicator of the vacancy concentration the width of the bright shell surrounding the reinforcement particle in Fig. 3, estimated to be,  $\Delta\rho_{\text{shell}} = 0.25$ . By replacing in (5),  $\rho_Y$  with 3.13 (see above),  $C_0$  with  $10^{-9}$  (Ref 35), and varying the value of  $k$ , until the predicted and the measured shell widths did match each other, it was obtained,  $k \approx 24.7$  (Note that this value is valid only for Al-5 wt.% TiCN.). The procedure of finding  $k$  is illustrated in Fig. 5, where three,  $C_v(\rho)$ , obtained by the varying of  $k$  are compared. As seen the selected value of  $k$  provides the best fit between the calculated and the experimental widths of the shell. Finally, solving  $k$  to  $\bar{E}_m(\bar{C}_v)$ , and replacing,  $\Delta\alpha = 2 \cdot 10^{-6}$  (Ref 25),  $\nu_{Al} = 0.345$  (Ref 26),  $\Delta T = 400$  K, and  $T = 300$  K, for the partial Young modulus of the matrix is obtained,  $\bar{E}_m(\bar{C}_v) = \frac{k(1+\nu)k_B T}{16\pi(\Delta\alpha\Delta T)^2 \langle r_p \rangle^3} = 4.21 \cdot 10^{-14} \langle r_p \rangle^{-3}$ . As seen,  $\bar{E}_m(\bar{C}_v)$  depends strongly on the reinforcement size, e.g., at  $\langle r_p \rangle = 1 \mu\text{m}$ ,  $\bar{E}_m(\bar{C}_v)$ ,  $\sim 4.21 \cdot 10^4$  Pa, while at  $\langle r_p \rangle = 10$  nm it is  $\bar{E}_m(\bar{C}_v) \sim 4.21 \cdot 10^{10}$  Pa. Notice, that with the reduction of the reinforcement size the partial Young modulus tends, as should be expected, to that of pure Al ( $E_{Al} = 7.6 \cdot 10^{10}$  (Ref 26)). The sharp decrease in,  $\bar{E}_m$ , with the increase in  $\langle r_p \rangle$ , influences negatively the strength of the composite because the weakening

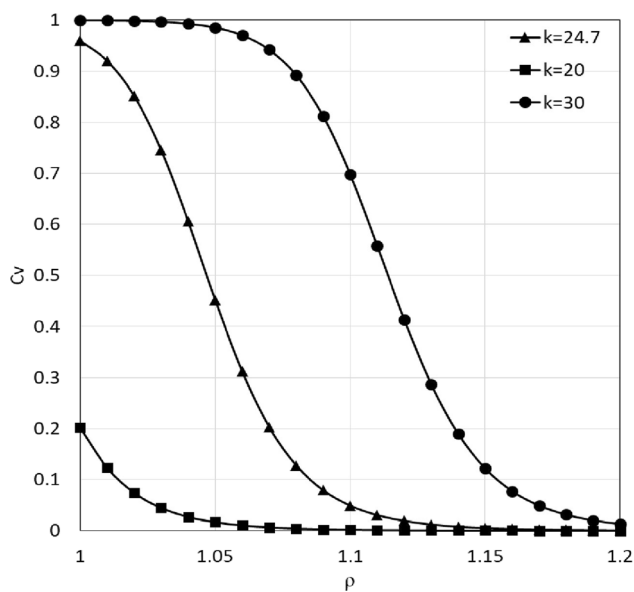


**Fig. 5** Plots of the vacancy concentrations  $C_v(\rho)$  (in fractions), calculated with Eq 5 for three different values of the parameter  $k$  (20, 24.7, and 30). Only the curve calculated with,  $k = 24.7$ , correctly predicts the thickness of the vacancy-rich shell (the bright halo around the particle in Fig. 3). The numerical data used in the calculations corresponds to that of a composite with 5 wt.% TiCN ( $f_v = 0.0306$ );  $\rho_Y = 3.13$ , and  $C_0 = 10^{-9}$ . The selection criterion, the thickness of the bright shell surrounding the in Fig. 3, was estimated to be,  $\Delta\rho_{\text{shell}} = 0.25$

takes place in the most vulnerable part of the composite, the reinforcement-matrix contact zone. Indeed, the replacement of matrix atoms with vacancies would lead to the rupturing of atomic/molecular bonds between the reinforcement and the matrix, thus resulting in a reduction of the adhesion force holding the composite together (cf. Fig. 2), whence a deterioration of the composite strength occurs. An estimate of the number of ruptured bonds shows that it depends on the  $C_v(\rho)|_{\rho=1}$  and  $\langle r_p \rangle$  being,  $n_{\text{ruptured}} = 4\pi\langle r_p \rangle^2 N_0 C_v(\rho)|_{\rho=1}$  (with  $N_0$  as the number of bonds per  $\text{m}^2$  in case of ideal, all bonds saturated, contact) (Ref 27, 36). One notes that the negative effect of increased vacancy concentration at the reinforcement-matrix boundary,  $C_v(\rho)|_{\rho=1}$ , is augmented with the increase in the reinforcement particle size. This result agrees with the conclusions drawn from the analysis of Fig. 2 and explains, why the larger reinforcement particles separate much more easily from the matrix while the smaller ones do not. It should be noted, however, that this negative effect of the reinforcement size, on the composite strength holds until the CTEM strengthening mechanism is inactive. After the critical reinforcement size is exceeded, the formation of dislocations begins, thus a part of the free volume concentrated in the vacancies is utilized in the growth of the dislocations generated by the stress field. As a consequence, a reduction of the vacancy concentration around the reinforcement occurs which benefits an increase in the Young modulus of the matrix near the reinforcement-matrix contact zone. Thus, the overall result of dislocations' increase and the reduction of the vacancy concentration is an improvement in the mechanical strength of the composite.

From the point of view of the composite's strength, i.e., when the composite is subjected to an external loading, the obtained results could be interpreted as follows: In the lower end of the reinforcement-sizes scale (i.e., nano-sizes),  $r_c/\langle r_p \rangle = 1$ , the stress generated by the CTEM in the matrix is low, therefore, the vacancy concentrations in the matrix around the reinforcement are also low thus the adhesion bonds, reinforcement-matrix, are preserved and are strong enough to keep the composite together. Therefore, it could be inferred that the decrease in the reinforcement's size has a positive effect on the composite's strength. With the increase in the reinforcement's size, due to the increase in the number of ruptured bonds, a deterioration of the strength conditions around the reinforcement occurs. At a reinforcement size of about a few microns, the number of ruptured bonds is at a maximum; while, CTEM strengthening is still non-operational. Therefore, it could be inferred that the reinforcement-matrix construct, respectively the mechanical strength of the composite, are in their most critical state. With the further increase in the reinforcement size, however, begins the nucleation of dislocations, which activates the CTEM strengthening mechanism. The generated dislocations serve as a sink to the vacancies, thus leading to a reduction of the vacancy concentration in the vicinity of the matrix-reinforcement contact zone, which further improves the mechanical strength of the composite.

The results obtained so far can be summarized as; when the size of the reinforcement is above the critical, CTEM has a positive effect on the strength of the composite, conversely, when this size is below the critical, the effect of CTEM on the strength of the composite is mostly negative, as it leads to an increased concentration of vacancies in the contact zone reinforcement-matrix and eventually to a reduction of adhesive forces. However, at the lower end of the particulates-sizes scale,

this negative effect is insignificant and is fully compensated by the increased strength of the adhesion forces.

## 4. Conclusions

CTEM strengthening originates from the differences in the thermal expansion coefficients and is presumed to be one of the major factors leading to the improvement of the mechanical properties of MMCs reinforced with micron- and nano-sized particulates. The analysis of the experimental data obtained in the present research and those of other researchers allows the conclusions:

- The CTEM strengthening effect is operational under certain temperatures, size of the reinforcement, and thermo-mechanical properties of reinforcement and matrix;
- The application of the CDLR theory, developed by Cottrell, to the problem studied, revealed that below a certain reinforcement size, it is impossible to nucleate dislocations thus making the CTEM strengthening non-operational;
- Cottrell's theory allowed drawing the following important conclusions; (i) the CTEM-generated dislocations nucleate predominantly in the vicinity of the reinforcements, and (ii) the size of the generated dislocations should be commensurate or smaller than the size of the reinforcement particle;
- The employment of the Einstein–Smoluchowski “drift-diffusion” equation allowed for explaining, how CTEM affects the mechanical strength of the composite when the CTEM strengthening mechanism is non-operational; The obtained results allowed for an explanation of the experimentally observed reduction of the adhesion force between the matrix and the reinforcement with the increase in the reinforcement size;
- Based on the results obtained, it was reasoned that a reinforcement size exists, evaluated to be  $\langle r_p \rangle \sim 1\text{-}3 \mu\text{m}$ , at which the positive effect of the particulate reinforcement on the mechanical strength of the composite is at its lowest. It was concluded that reducing the size of reinforcement particles from micron- to nano-scale sizes improves the reinforcement's performance as a strengthening factor.

## Acknowledgments

The financial support of the present research by the European Regional Development Fund - BG05M2OP001-1.001-0008-C08, and Bulgarian National Foundation of Science and Research NFNI-Project DH 07/16, are gratefully acknowledged.

## Appendix

The proof of Young modulus dependency on the vacancy concentration we start with the thermodynamical identities:

$$F = G \left( u_{ik} - \frac{1}{3} u_{ll} \delta_{ik} \right)^2 + \frac{1}{2} K u_{ll}^2 \quad (\text{Eq A.1})$$

and

$$F_{\text{mol}} = \mu_m(1 - C_v) + \mu_v C_v. \quad (\text{Eq A.2})$$

Where  $u_{ik}$  are components of the strain tensor,  $\mu_m$  and  $\mu_v$  are the chemical potentials of the matrix and the vacancies in the matrix-vacancy solution, and  $G$  and  $K$  are the shear and bulk moduli.

At an arbitrary deformation of the matrix-vacancy solution is valid:

$$\mu_m = \bar{G}_m \left( u_{ik} - \frac{1}{3} u_{ll} \delta_{ik} \right)^2 + \frac{1}{2} \bar{K}_m u_{ll}^2 \quad \text{and} \\ \mu_v = \bar{G}_v \left( u_{ik} - \frac{1}{3} u_{ll} \delta_{ik} \right)^2 + \frac{1}{2} \bar{K}_v u_{ll}^2, \text{ after replacing in (A.2) and rearranging the members is obtained:}$$

$$\left( G - \bar{G}_m(1 - C_v) - \bar{G}_v C_v \right) \left( u_{ik} - \frac{1}{3} u_{ll} \delta_{ik} \right)^2 \\ + \frac{1}{2} \left( K - \bar{K}_m(1 - C_v) - \bar{K}_v C_v \right) u_{ll}^2 = 0.$$

Because  $\left( u_{ik} - \frac{1}{3} u_{ll} \delta_{ik} \right)^2$  and  $u_{ll}^2$  are arbitrary quantities the above identity could be valid only in the case of:

$$G = \bar{G}_m(1 - C_v) + \bar{G}_v C_v \text{ and } K = \bar{K}_m(1 - C_v) + \bar{K}_v C_v.$$

We recall that  $G$  and  $K$  could be expressed with the Young modulus  $E$  and the Poisson ratio  $\nu$  as,  $G = \frac{E}{2(1+\nu)}$  and  $K = \frac{E}{3(1-2\nu)}$ , whence:

$$\frac{E}{2(1+\nu)} = \frac{\bar{E}_m}{2(1+\nu_m)}(1 - C_v) + \frac{\bar{E}_v}{2(1+\nu_v)} C_v. \quad (\text{Eq A.3})$$

The fraction of the vacancies in the matrix is negligible,  $C_v \sim 10^{-8}\text{-}10^{-10}$ , thence, by taking into account that the Poisson ratio of the matrix of the materials is,  $\nu \in \{1/4..1/2\}$ , it could be accepted that the denominators in (A.3) are equal, thus:

$$E = \bar{E}_m(1 - C_v) + \bar{E}_v C_v \quad (\text{Eq A.4})$$

Further, due to the reasons above, the second member of the right-hand side of (A.4) could be neglected thus leading to  $E = \bar{E}_m(1 - C_v)$ .

## References

1. M. Taya and R.J. Arsenault, *Metal Matrix Composites – Thermo-mechanical behavior*, Pergamon Press, Pergamon, 1989
2. A.R.T. de Silva, and G.D. Chadwick, Thermal, Stresses in Fiber Reinforced Composites, *J. Mech. Phys. Solids*, 1969, **17**, p 387–403
3. J. Humphreys and P.B. Hirsch, The Deformation of Single Crystals of Copper and Copper-Zinc Alloys Containing Alumina Particles II. Microstructure and Dislocation-Particle Interactions, *Proc. Royal Soc. (London) A*, 1970, **318**, p 73–92
4. P.M. Hazzledine and P.B. Hirsch, A Coplanar Orowan Loops Model for Dispersion Hardening, *Phil. Mag.*, 1974, **30**, p 1331–1351
5. M. Taya and T. Mori, Dislocations Punched Out Around a Short Fiber in a Short Fiber Metal Matrix Composite Subjected to Uniform Temperature Change, *Acta Metall.*, 1987, **35**, p 155–162
6. D. Dunand and A. Mortensen, Thermal Mismatch Dislocations Produced by Large Particles in a Strain-Hardening Matrix, *Mat. Sci. Eng. A.*, 1991, **135**, p 179–184
7. R. Vogt, Z. Zhang, Y. Li, M. Bonds, N.D. Browning, E.J. Lavermia, and J.M. Schoenung, The Absence of Thermal Expansion Mismatch Strengthening in Nanostructured Metal–Matrix Composites, *Scripta Mater.*, 2009, **61**, p 1052–1055
8. Sh. Dong, J. Zhou, D. Hui, Y. Wang, and S. Zhang, Size-Dependent Strengthening Mechanisms in Carbon Nanotube Reinforced Metal Matrix Composites, *Compos. Part A Appl. Sci. Manuf.*, 2015, **68**, p 356–364



9. L. Anestiev, Part II: Strengthening and Strength-Reduction at MMCs Reinforced with Nano-Sized Particulates, *Aluminum surface and bulk nanocomposites*. R. Lazarova, L. Anestiev Ed., Cambridge Scholars Publications, Newcastle upon Tyne, 2022
10. E. Orowan, Mechanische Festigkeitseigenschaften und die Realstruktur der Kristalle, *Z. Kristallogr.*, 1934, **89**, p 327–343. (in German)
11. L. Anestiev, R. Lazarova, P. Petrov, V. Dyakova, and L. Stanev, On the Strengthening and the Strength Reducing Mechanisms at Aluminum Matrix Composites Reinforced with nano-Sized TiCN Particulates, *Philos. Mag.*, 2021, **101**(2), p 129–153
12. V. Dyakova, Institute of Metal Science, Equipment and Technologies with Center for Hydro- and Aerodynamics, Sofia, Bulgaria, 2019 and 2020
13. N.E. Dowling, *Mechanical Behavior of Materials Engineering: Methods for Deformation, Fracture, and Fatigue*, 4th ed. Pearson Education Ltd., London, 2013
14. Mitchell, in Growth, and Perfection of Crystals, Proceedings of an International Conference on Crystal Growth, August 27-29, (Cooperstown, New York), John Wiley & Sons, 1958, p. 386,
15. D. Hull and D.J. Bacon, *Introduction to Dislocations*, 5th ed. Elsevier, Butterworth-Heinemann, 2011
16. R.M. Jones, *Deformation Theory of Plasticity*, Bull Ridge Publishing, Blacksburg, Virginia, 2009
17. S.P. Timoshenko and J.N. Goodier, *Theory of Elasticity*, 3rd ed. McGraw-Hill, New York, 1970
18. R.W.K. Honeycombe, *The Plastic Deformation of Metals*, Edward Arnolds Publ. Ltd., London, 1968
19. A.H. Cottrell, Theory of Dislocations, *Progress Metal Phys.*, 1953, **4**, p 205–264. [https://doi.org/10.1016/0502-8205\(53\)90018-5](https://doi.org/10.1016/0502-8205(53)90018-5)
20. A.H. Cottrell, *Dislocations and plastic flow in crystals*, Oxford University Press, Oxford, 1953
21. F.R.N. Nabarro, The Mathematical Theory of Stationary Dislocations, *Adv. Phys.*, 1952, **1**, p 271
22. D. Kuhlmann-Wilsdorf, Dislocations, Physical Metallurgy, R. W. Cahn Ed., (Amsterdam), North-Holland Publ., 1965, Chapter 13
23. E. Schmid and W. Boas, *Plasticity of Crystals with Special Reference to Metals*, F. A. Hughes & Co. Ltd, London, 1950
24. R. Faulkner and J. Martin, *Dislocation Theory for Engineers: Worked Examples*, Alden Press, Oxford, 2000
25. R. Stylianou, D. Velic, W. Daves, W. Ecker, A. Stark, N. Schell, M. Tkadletz, N. Schalk, Ch. Czettl, and Ch. Mitterer, Stress Relaxation through Thermal Crack Formation in CVD TiCN Coatings Grown on WC-Co with Different Co Contents, *Int. J. Refract. Met. H.*, 2020, **86**, 105202
26. E.A. Brandes and G.B. Brook Eds., *Smithells Metals Reference Book*, 7th ed. Butterworth-Heinemann, Oxford, 1999
27. D.M. Jarzabek, M. Chmielewski, J. Dulnik, and A. Strojny-Nedza, The Influence of the Particle Size on the Adhesion Between Ceramic Particles and Metal Matrix in MMC Composites, *J. Mater. Eng. Perform.*, 2016, **25**(8), p 3139–3145
28. L.D. Landau and E.M. Lifshitz, *Statistical Physics*, Elsevier, Butterworth-Heinemann, 2005
29. A. Sommerfeld, *Lectures on Theoretical physics*, Vol 5 Academic Press, New York, 1954
30. , L. S. Darken and R. W. Gurry, Physical Chemistry of Metals, McGraw-Hill series in materials science and engineering, McGraw-Hill, 1953
31. G. Shewmon Saul, *Diffusion in solids*, McGraw-Hill, New York, 1963
32. H. Mehrer, *Diffusion in Solids*, Springer Berlin Heidelberg, Berlin, Heidelberg, 2007
33. A. Münster, *Chemische Thermodynamik*, De Gruyter, 1969. <https://doi.org/10.1515/9783112479186>
34. Y. Sun, Lu. Cheng, Yu. Hailiang et al., Nanomechanical Properties of TiCN and TiCN/Ti Coatings on Ti Prepared by Filtered Arc Deposition, *Mater. Sci. Eng. A*, 2015, **625**, p 56–64. <https://doi.org/10.1016/j.msea.2014.11.093>
35. R.W. Siegel, Vacancy Concentrations in Metals, *J. Nucl. Mater.*, 1978, **69**, p 117–146
36. A.P. Boresi and R.J. Schmidt, *Advanced mechanics of materials*, 6th ed. John Wiley & Sons, Inc., New York, 2003

**Publisher's Note** Springer Nature remains neutral with regard to jurisdictional claims in published maps and institutional affiliations.

Springer Nature or its licensor (e.g. a society or other partner) holds exclusive rights to this article under a publishing agreement with the author(s) or other rightsholder(s); author self-archiving of the accepted manuscript version of this article is solely governed by the terms of such publishing agreement and applicable law.